Title: *Limosilactobacillus reuteri*-derived tripeptide SKL exerts antibacterial activity against systemic and wound infections via dual membrane-killing and anti-virulence mechanisms

Authors: Qi Lu [a, b], Di Wang [a], Haojie Jing [a], Haijian Wang [a, b], Na Li [a], Baikui Wang [a, c], Longhai Yu [a], Yifei Feng [a, b], Liyuan Mo [a], Kun Zhou [a], Min Yue [a, c], Yan Li [a, b*]

Affiliations:

a MOA Key Laboratory of Animal Virology & Zhejiang Provincial Engineering Research Center of Animal Biological Products, Zhejiang University College of Animal Sciences, Hangzhou, Zhejiang 310058, China

b Hainan Institute of Zhejiang University, Sanya, Hainan 572025, China

c Key Laboratory of Systems Health Science of Zhejiang Province, School of Life Science, Hangzhou Institute for Advanced Study, University of Chinese Academy of Sciences, Hangzhou, Zhejiang 310024, China

*Corresponding author: Yan Li, yanli3@zju.edu.cn

This version supersedes all previous versions regarding the updated terms.

ABSTRACT

The escalating crisis of antimicrobial resistance (AMR) necessitates innovative antimicrobial strategies beyond conventional antibiotics. Although the beneficial effects of probiotics are well recognized, the specific molecular effectors responsible for their systemic protective functions remain largely unexplored. Here, we screened the piglet gut microbiota and identified *Limosilactobacillus reuteri* P190 as a strain with potent, broad-spectrum activity against diverse bacterial pathogens and robust protection against lethal systemic *Salmonella* infection *in vivo*. Mechanistic investigations revealed that this protective effect is attributed to a novel tripeptide, Ser-Lys-Leu (SKL). SKL exerts a unique dual mode of action: it rapidly disrupts bacterial cell membranes at inhibitory concentrations, while simultaneously attenuating virulence by targeting the QseC quorum-sensing system even at sub-inhibitory concentrations. Notably, through tandem-repeat engineering, we developed a highly potent variant, $(SKL)_4$, which dramatically enhances direct antimicrobial efficacy while retaining low hemolysis and cytotoxicity. Both SKL and $(SKL)_4$ protect mice from lethal systemic *Salmonella* challenges independent of host immunity, demonstrating their direct, autonomous therapeutic power. Furthermore, topical applications of these peptides successfully cleared methicillin-resistant *Staphylococcus aureus* wound infections and accelerated healing, with efficacy comparable to that of mupirocin. Collectively, our findings identify SKL as a promising probiotic-derived lead antimicrobial peptide with dual membrane-disrupting and anti-virulence capabilities, offering a compelling strategy to combat multidrug-resistant pathogens.

KEYWORDS: Gut microbiome; *Limosilactobacillus reuteri*; tripeptide SKL; antimicrobial peptide (AMP); QseC

Introduction

Antimicrobial resistance (AMR) remains one of the most urgent threats to global health. According to the most recent comprehensive global estimate, bacterial AMR was estimated to have directly caused 1.14 million deaths and to have been associated with an additional 4.71 million deaths; by 2050, these numbers are projected to increase to 1.91 million and 8.22 million, respectively.[1] The growing burden is driven by clinically important resistant pathogens that continue to undermine the efficacy of existing antibiotics and expose the limitations of current antibacterial development pipelines. These challenges underscore the urgent need for new antibacterial agents and innovative therapeutic strategies to solve antibiotic resistance.[1, 2]

Antimicrobial peptides (AMPs) have emerged as promising next-generation anti-infective agents.[3] Unlike many conventional antibiotics which typically act on specific enzymatic or biosynthetic targets, AMPs often exert rapid and broad-spectrum activity by disrupting bacterial membranes.[4, 5] Their cationic and amphipathic properties promote preferential interactions with bacterial envelopes, resulting in membrane destabilization, depolarization, pore formation, and leakage of intracellular contents.[5, 6] Although AMPs are generally considered less susceptible to classical resistance, bacterial envelope remodeling and other adaptive responses can still diminish AMP activity *in vivo*.[4, 7] Therefore, a pressing need remains to discover and characterize novel AMPs to combat the growing threat of antimicrobial resistance.

The host-associated microbiome represents an evolutionarily selected reservoir of bioactive molecules shaped by ecological competition, microbial coexistence, and host adaptation.[8, 9] Machine-learning approaches have recently enabled the prediction and identification of active AMPs from both the human gut microbiome and global microbial metagenomes.[10, 11] Among gut commensals, probiotic lactic acid bacteria (LAB) are recognized as producers of diverse antimicrobial metabolites, and large-scale genomic mining coupled with machine learning has further expanded the repertoire of LAB-derived AMPs.[12] However, due to their cationic and amphipathic

nature, AMPs are often associated with adverse effects such as hemolysis or nephrotoxicity, with stronger bactericidal activity frequently correlating with a greater propensity for off-target toxicity.[13] Most high-throughput screening platforms prioritize direct bactericidal activity and in vitro potency, while the *in vivo* effects, including suppression of virulence, biofilm formation, and antibody-assisted bacterial clearance, as well as adverse effects, are often undetermined.[14-16]

Here, we identified a probiotic-derived tripeptide, SKL, with broad antibacterial activity isolated from piglet gut microbes. Tandem-repeat engineering optimized it into $(SKL)_4$, showing enhanced charge, structure, and potency with host safety. Both SKL and $(SKL)_4$ exert rapid bactericidal effects via membrane disruption; SKL also inhibits virulence by downregulating QseC, thereby impairing biofilm formation. In murine models of both systemic and localized infection, SKL and $(SKL)_4$ significantly reduced bacterial burdens and improved disease outcomes without overt toxicity. Thus, SKL is a microbiome-derived lead AMP that integrates direct membrane-targeted killing with targeted anti-virulence activity, highlighting the value of ecological discovery and rational engineering for antimicrobial development.

Materials and Methods

Bacterial strains and culture conditions

A complete list of bacterial strains and culture conditions is provided in Supplementary Methods. In brief, *Salmonella* Typhimurium SL1344 and the other bacterial strains used in this study were maintained under species-appropriate growth conditions.

Antimicrobial peptide characterization and in vitro assays

The identification of the secreted tripeptide SKL, synthesis of tandem-repeat derivatives, and all in vitro antimicrobial assays, including MIC/MBC determination, time-kill kinetics, hemolysis, mammalian cell viability, biofilm inhibition, resistance passage, and membrane-damage assays, are described in Supplementary Methods.

Mouse experiments

All animal procedures were approved by the Institutional Animal Care and Use Committee of Zhejiang University and were performed under Animal Biosafety Level 2 (ABSL2) containment. Mice were housed under specific-pathogen-free conditions with free access to sterile water and autoclaved chow.

For the systemic *Salmonella* infection model, C57BL/6 mice received P190, P190 cell-free supernatant, or protease-digested supernatant before and after oral challenge with *S.* Typhimurium SL1344, whereas SKL and $(SKL)_4$ were evaluated in separate prophylactic and therapeutic regimens via the indicated routes of administration. Mice were monitored for body weight, survival, and bacterial burden in target organs at the indicated time points. To determine whether peptide activity required host immunity, a cyclophosphamide-induced neutropenic mouse model was used. To assess whether the in vivo effect of SKL was mediated by microbiota remodeling, a fecal microbiota transplantation experiment was performed. To verify QseC-dependent virulence suppression in vivo, a competitive infection assay using a

1:1 mixture of wild-type and *ΔqseC S.* Typhimurium was conducted. For localized infection, BALB/c mice were used in a full-thickness MRSA wound infection model and treated topically with SKL ointment, $(SKL)_4$ ointment, mupirocin, or vehicle control. Detailed protocols for each animal model are provided in Supplementary Methods.

Generation of *qseC* knockout and complemented strains

The *qseC* deletion mutant (*ΔqseC*) was constructed using the pCas/pTarget CRISPR-Cas9-assisted λ Red recombination system, and the complemented strain (C-*ΔqseC*) was generated by introducing a pACYC184-based plasmid carrying the *qseC* gene with its native promoter into the *ΔqseC* mutant. Detailed procedures are provided in Supplementary Methods.

qRT-PCR and Western blot analysis

Quantitative real-time PCR, bacterial protein extraction, Western blot analysis, and primer information are described in Supplementary Methods.

Statistical analysis

Statistical analysis is described in Supplementary Methods.

Result

Gut-derived *Limosilactobacillus reuteri* P190 confers protection against systemic *Salmonella* infection in mice

The healthy livestock gut harbors a rich community of symbiotic microbes with documented probiotic potential.[17] Among these, gut-derived LAB are particularly well-adapted to the host environment and have been shown to counteract bacterial infections through the production of broad-spectrum antimicrobial metabolites.[18] From the intestinal contents of one-month-old healthy piglets, we isolated 750 bacterial strains, of which 325 were identified as LAB by matrix-assisted laser desorption/ionization time-of-flight mass spectrometry (MALDI-TOF MS), including 26 strains of *Limosilactobacillus reuteri* **(Figure 1a)**. Using an agar well-diffusion assay, we screened all 325 LAB isolates for antibacterial activity **(Supplemental Table S1).** All 26 *L. reuteri* strains exhibited activity against a panel of clinically relevant pathogens (*Enterococcus faecium*, *Staphylococcus aureus*, *Klebsiella pneumoniae*, *Acinetobacter baumannii*, *Pseudomonas aeruginosa*, and *Salmonella* Typhimurium) with a general preference for Gram-negative over Gram-positive bacteria. Among these strains, strain P190 displayed the strongest inhibitory effect, whereas strain P126 showed the weakest **(Figure 1b)**. Notably, P190 was the most potent inhibitor of *Salmonella* Typhimurium of the set.

Encouraged by the robust *in vitro* activity of P190 against *S.* Typhimurium, we next assessed its protective efficacy *in vivo* using a mouse model of systemic *S.* Typhimurium infection. C57BL/6 mice orally received P190 or PBS daily for 7 days prior to *S.* Typhimurium infection, with treatments continuing thereafter **(Figure 1c)**. Whereas all PBS-treated control mice succumbed to infection by day 7, showing rapid and severe weight loss, P190-treated mice exhibited significantly prolonged survival, with 30% (3/10) still alive at 20 days post-infection (dpi) **(Figures 1d, 1e)**. At 3 dpi, *S.* Typhimurium colony-forming units (CFUs) recovered from liver, spleen, and cecal contents of P190-treated mice were 4-126 times fewer than from PBS-treated mice. Furthermore, only 2 of 6 blood samples from P190-treated mice had detectable

bacteria, and those counts approached the detection limit **(Figure 1f)**.

Histological examination of liver and spleen at 3 dpi corroborated these findings. Compared with mock-infected control mice, PBS-treated mice displayed severe organ damage: livers showed disrupted architecture and widespread inflammatory foci, while spleens exhibited extensive structural disorganization, sparse white-pulp lymphocytes, heavy neutrophil infiltration of the red pulp, and diffuse lymphocyte necrosis. In contrast, P190-treated mice developed only mild inflammatory changes in both liver and spleen, with no obvious tissue necrosis or architecture disruption **(Figures 1g, 1h)**. Collectively, these results demonstrate that *L. reuteri* P190 confers potent protection against systemic *S.* Typhimurium SL1344 infection in mice.

The secreted tripeptide SKL is the principal antimicrobial effector of *L. reuteri* P190

To pinpoint the active antibacterial component of *L. reuteri* P190, we first separated the whole culture into a bacteria-free supernatant and a bacteria pellet and tested each fraction against *S.* Typhimurium SL1344 using an agar diffusion assay. Strong antimicrobial activity was observed in both the whole culture and the supernatant, but not in the pellet **(Figure 2a)**, indicating that the primary antibacterial effector is a secreted metabolite rather than bacterial cells or their structural components.

We next characterized the biochemical nature of this effector. Untreated supernatant completely inhibited bacterial growth within 2-4 hours. This activity was markedly reduced by treatment with trypsin but unaffected by pepsin **(Figures 2b, 2c)**, suggesting that the active factor is a peptide or protein sensitive to trypsin yet resistant to gastric pepsin. In a mouse model of *S.* Typhimurium infection, untreated P190 supernatant significantly improved survival and lowered bacterial loads, whereas trypsin pretreatment eliminated these effects (**Figures 2d-2g**), confirming the peptide-dependent protection *in vivo*.

To identify the specific antibacterial peptide, we fractionated the P190 supernatant. Antimicrobial activity was observed exclusively in the <3 kDa fraction **(Figure S1a)**

and was protease-sensitive **(Figures S1b and S1c)**, indicating that the activity was attributable to a small peptide. Untargeted metabolomics was then performed on P190 supernatant, with P126 as a control. Principal component analysis (PCA) revealed clear separation of the two metabolomes **(Figure 2h)**, indicating distinct metabolite profiles. Of 716 differentially expressed metabolites, 278 were upregulated and 438 were downregulated in P190 **(Supplemental Table S2)**. Amino acids and their derivatives (58 metabolites) and organic acids and derivatives (42 metabolites) were the most abundant categories **(Figure 2i)**, consistent with the observation that NaOH neutralization reduced antibacterial activity **(Figure S1d, S1e)**. Among upregulated amino-acid-related differentially expressed metabolites ($\log_2$ fold change > 1), only two peptides longer than two residues were found: the tripeptides Ala-Pro-Lys (APK) and Ser-Lys-Leu (SKL) **(Figure 2j)**. Structural and sequence analysis of SKL predicted a cleavage site for trypsin but no canonical pepsin cleavage motif **(Figure 2k, 2l)**. Notably, SKL showed broad-spectrum activity against a panel of clinically relevant Gram-negative and Gram-positive pathogens **(Figure S2a)**, with a minimum inhibitory concentration (MIC) of 128 μg/mL against *S.* Typhimurium SL1344 **(Figure 2m)**. Trypsin treatment raised the MIC to 256 μg/mL, whereas pepsin had no effect **(Figure 2m)**. APK, in contrast, exhibited substantially weaker activity, with MIC values ranging from 2.5 to 10 mg/mL against the tested pathogens **(Figures S2b, S2c)**, and its MIC remained unchanged upon trypsin or pepsin treatment **(Figure S2d)**. Together, these data identify tripeptide SKL as the principal antimicrobial peptide secreted by *L. reuteri* P190.

Tandem-repeat optimization of SKL enhances antimicrobial activity

The tripeptide SKL showed only modest activity against *S.* Typhimurium (MIC = 128 μg/mL), considerably weaker than polymyxin B, which typically exhibits MIC values of 0.25–2 μg/mL against most susceptible Gram-negative pathogens.[19] To improve its potency, we turned to rational design. SKL carries a positive charge and hydrophobic residues, which are characteristic of antimicrobial peptides and facilitate binding to negatively charged bacterial membranes. Moreover, its C-terminal leucine is known to

stabilize α-helical structure in amphipathic AMPs.[20] We reasoned that the short length of the tripeptide limited its charge density, amphipathicity, and helical stability. Accordingly, we synthesized tandem repeats of the SKL motif in 3, 4, 5, 6, or 9 copies (designated $(SKL)_3$ - $(SKL)_9$) via solid-phase synthesis to augment net cationic charge and hydrophobic moment while promoting α-helix formation via the repeating leucine residues. AlphaFold secondary-structure prediction confirmed stable α-helices in all constructs **(Figure 3a)**, supporting our design rationale.

We next evaluated the antimicrobial activity of the SKL repeats against 17 bacterial strains, including Gram-negative and Gram-positive pathogens, as well as probiotic lactobacilli. $(SKL)_4$ and $(SKL)_5$ reduced the MIC against *S.* Typhimurium SL1344 to 8 μg/mL, equivalent to a 16-fold improvement over native SKL **(Figure 3b)**. However, further extension to 6 or 9 copies did not enhance antimicrobial potency; instead, the MIC increased for most strains **(Figure 3b)**, suggesting the optimal peptide length is critical for maintaining antimicrobial efficacy. Notably, all repeats displayed broad-spectrum activity but were more potent against Gram-negative (MIC 8-64 μg/mL) than against Gram-positive bacteria (MIC 32-128 μg/mL). Inhibitory activity against *L. reuteri* P190 and other lactobacilli was minimal (MIC > 256 μg/mL). Biocompatibility testing revealed low hemolysis (<2%) and high mammalian cell viability (>95%) for SKL, $(SKL)_3$, and $(SKL)_4$, whereas $(SKL)_5$ and longer repeats caused increased hemolysis and reduced viability **(Figure 3c)**. Time–kill assays against *S.* Typhimurium SL1344 showed that $(SKL)_4$ achieved complete bacterial clearance at 1×MBC within 1.5 hours, compared to 9 hours for SKL **(Figure 3d)**, indicating that $(SKL)_4$ achieved markedly faster bactericidal kinetics. Based on these results, we selected $(SKL)_4$ for further characterization.

Lastly, we tested the likelihood of resistance emergence by passaging *S.* Typhimurium and methicillin-resistant *S. aureus* (MRSA) to 20 passages in subinhibitory concentrations (½×MIC) of SKL or $(SKL)_4$, with polymyxin B and vancomycin as controls. No MIC increase was observed for either SKL or $(SKL)_4$ after 20 passages, whereas MICs for polymyxin B and vancomycin rose 32-fold and 8-fold, respectively **(Figures 3e, 3f)**. Thus, tandem-repeat optimization enhances bactericidal

potency without driving rapid resistance, consistent with the known low resistance propensity of membrane-active AMPs.[21 22]

SKL and $(SKL)_4$ specifically disrupt bacterial cell membranes

The cationic and amphipathic nature of SKL and $(SKL)_4$ suggests a membrane-disruptive mechanism, similar to that of antimicrobial peptides. To visualize this, we examined treated bacterial cells using scanning electron microscopy (SEM). Exposure to SKL or $(SKL)_4$ at 1×MIC for 1 hour caused severe morphological alterations, including cell shrivelling, surface irregularities, and the formation of membrane ruptures and holes. This structural damage was more pronounced with $(SKL)_4$ treatment than with SKL **(Figure 4a)**. Likewise, MRSA cells displayed distinct membrane distortions and leakage of intracellular contents following treatment with SKL or $(SKL)_4$ **(Figure 4a)**.

Membrane permeabilization was further quantified via fluorescence assays. SLK and $(SKL)_4$ gradually increased the N-phenyl-1-naphthylamine (NPN) fluorescence intensity, and they elicited a 20-fold increase in NPN fluorescence intensity relative to the PBS vehicle following a 6-hour treatment, demonstrating a substantial increase in the outer-membrane (OM) permeability of *S.* Typhimurium post SKL- and $(SKL)_4$ treatment **(Figure 4b)**. Moreover, a significant rise in inner-membrane (IM) permeability was observed as early as 60 minutes for SKL and 40 minutes for $(SKL)_4$, with the permeability peaking at 120 minutes for SKL and at 80 minutes for $(SKL)_4$. In both assays, $(SKL)_4$ induced greater membrane permeability than SKL **(Figure 4c)**. Consistent with these findings, SKL and $(SKL)_4$ triggered rapid leakage of intracellular nucleic acids and proteins, with $(SKL)_4$ mediating a faster efflux rate **(Figures 4d, 4e).** Notably, the membrane-disruptive potency of $(SKL)_4$ was comparable to that of polymyxin B **(Figures S3a, S3b)**.

Furthermore, SKL and $(SKL)_4$ treatment significantly altered the biophysical properties of the bacterial membrane, characterized by increased fluidity and decreased hydrophobicity compared to vehicle controls **(Figures 4f, 4g)**. Reduced

membrane hydrophobicity compromises structural stability, while elevated fluidity disrupts membrane order; these synergistic effects undermine membrane integrity[23] and facilitate the observed cellular leakage. Together, these data confirm that SKL and $(SKL)_4$ kill bacteria by disrupting membrane integrity, aligning with the established mechanism of membrane-active antimicrobial peptides.

SKL and $(SKL)_4$ protect mice from systemic *Salmonella* infection independent of host immunity

Having established the *in vitro* potency of SKL and $(SKL)_4$, we next assessed their therapeutic potential *in vivo* using murine models of systemic *S.* Typhimurium infection. Dose optimization in immunocompetent C57BL/6 mice revealed that a single daily intraperitoneal (i.p.) injection of 25 mg/kg SKL for 3 days reduced bacteria loads in the liver, spleen, and blood to below the limit of detection; cecal *S.* Typhimurium CFUs were 5000 times lower than those in vehicle-treated controls **(Figures S4a, S4b)**. While oral gavage required a higher dose (50 mg/kg) to achieve comparable efficacy **(Figure S4c)**, i.p. 25 mg/kg $(SKL)_4$ was sufficient to clear systemic infection **(Figure S4d)**. At this optimized dose, both peptides rescued mice from lethal infection, mitigating weight loss and improving 20-day survival to 60% with SKL and 80% with $(SKL)_4$, whereas all vehicle-treated control mice succumbed within one week **(Figures S4e, S4f)**. Histological examination of liver and spleen at 3 dpi revealed that compared to mock mice, vehicle-treated mice displayed extensive hepatic and splenic destruction with rampant inflammation, whereas SKL- and $(SKL)_4$-treated mice retained largely normal organ architecture, including intact hepatocyte nuclei, well-formed hepatic cords, and spleens with preserved follicles and clear red/white pulp boundaries, with only minimal focal inflammation **(Figures S4g, S4h)**. Importantly, serum alanine aminotransferase (ALT) and blood urea nitrogen (BUN) levels remained unchanged relative to vehicle-treated controls, indicating this protection occurred without hepatotoxicity or nephrotoxicity **(Figures S5a, S5b)**. We also tested prophylactic administration: pre‑infection treatment with either peptide produced

similar outcomes, reducing bacterial loads in the liver, spleen, and cecal contents to approximately 1.6%–5% of vehicle control levels and extending survival by 3–10 days **(Figures S6a-c)**, confirming that SKL and $(SKL)_4$ confer robust therapeutic and prophylactic protection against systemic *Salmonella* infection.

To determine whether this protection arises from direct antimicrobial action rather than host-mediated effects, we evaluated peptide efficacy in a neutropenic mouse model. Flow cytometry analysis confirmed that cyclophosphamide pretreatment significantly depleted peripheral blood $CD8^+$ T cells, B cells, and neutrophils compared to untreated controls **(Figures S7a, S7b)**. Cyclophosphamide-pretreated mice were infected with *S.* Typhimurium and administered 25 mg/kg SKL, $(SKL)_4$, or vehicle via i.p. injection at 2 h, 24 h, and 48 h post-infection **(Figure 5a)**. While all PBS-treated mice died by day 5, peptide-treated mice showed attenuated weight loss and significantly extended survival, with 30% of mice surviving to the end of the observation period **(Figures 5b, 5c)**. At 2 dpi, SKL- and $(SKL)_4$-treated mice harbored 126-3162 times fewer *S*. Typhimurium CFUs in the liver, spleen, and cecum; blood bacterial loads fell to near the detection limit, whereas vehicle-treated mice exhibited severe bacteremia **(Figure 5d)**. These data confirmed that SKL and $(SKL)_4$ protect mice from systemic bacterial infection independent of host immunity.

Finally, to exclude indirect protection mediated by microbiota remodeling, we performed fecal microbiota transplantation. Recipient mice colonized with microbiota from SKL-treated donors showed no survival advantage or reduction in tissue bacterial loads following *S.* Typhimurium infection compared to recipients of vehicle-treated microbiota **(Figures S8a-c)**. Thus, the *in vivo* efficacy of SKL and $(SKL)_4$ is not mediated by shifts in microbial community but rather reflects direct antibacterial activity. This result excludes major microbiota-mediated effects and confirms that SKL's *in vivo* efficacy is principally due to its direct antimicrobial action. Intriguingly, while $(SKL)_4$ exhibits superior membrane disruption and antimicrobial activity *in vitro*, SKL and $(SKL)_4$ confer equivalent protection *in vivo*, suggesting that SKL may regulate specific signaling pathways that compensate for its lower direct lytic activity.

SKL suppresses virulence by targeting the QseC quorum-sensing system

Bacterial biofilm formation drives antibiotic resistance and persistent infection.[24] We therefore tested whether SKL and $(SKL)_4$ inhibit *S.* Typhimurium biofilm formation. SKL significantly inhibited *Salmonella* biofilm formation even at subinhibitory concentration (¼×MIC). Although $(SKL)_4$ achieved biofilm eradication at 1×MIC comparable to polymyxin B at 4×MIC, it failed to reduce biofilm formation at ¼×MIC **(Figure 6a)**. This ¼×MIC concentration is well below the MIC of SKL and insufficient to exert direct bactericidal effects, suggesting that SKL possesses unique subinhibitory mechanisms that $(SKL)_4$ lacks, possibly linked to the regulation of biofilm formation.

Given that biofilm formation is regulated by amino-acid-sensing signaling,[25] we screened four well-known bacterial signaling systems that sense amino acid or peptide signals to regulate biofilm formation and virulence: QseB/QseC,[26] PhoP/PhoQ,[27, 28] Lrp,[29] and CpxA/CpxR.[30] Quantifying the transcription of their central regulator (*qseC*, *phoP*, *lrp*, *cpxA*) revealed that only *qseC* was significantly downregulated by SKL **(Figure 6b)**. At 1×MIC, SKL reduced *qseC* mRNA levels by ~84.5% in *S.* Typhimurium SL1344, whereas *phoP*, *lrp*, and *cpxA* expression remained unchanged **(Figure 6b)**. Importantly, the tetramer $(SKL)_4$, which lacks biofilm-inhibitory activity at subinhibitory concentrations, did not affect *qseC* expression, establishing a strong correlation between QseC modulation and biofilm formation phenotype. Dose-response analysis showed that SKL at ¼×MIC, ½×MIC and 1×MIC progressively lowered *qseC* transcript levels **(Figure 6c)**. At ¼×MIC of SKL, *qseC* mRNA level fell by ~62.2%, and biofilm formation was similarly reduced **(Figure 6a)**. This parallel dose-dependency suggested a causal relationship between QseC suppression and the anti-biofilm activity of SKL. Western Blot confirmed that SKL markedly reduced QseC protein abundance of *S.* Typhimurium **(Figure 6d)**. To confirm the specificity of SKL on QseC, we generated a strain with *qseC* knockout (*ΔqseC*) and a complemented strain (C-*ΔqseC*) in the background of *S.* Typhimurium SL1344. QseC was absent in the *ΔqseC* regardless of SKL treatment, whereas C-*ΔqseC* recapitulated the response of the wild-type (WT) strain, showing 31.4% reduction in QseC protein levels after SKL treatment. These data identify QseC as the target through which SKL disrupts biofilm formation

and virulence.

QseC is a histidine kinase in the QseB/QseC two-component system that phosphorylates the response regulator QseB to regulate key virulence traits,[26] including genes from *Salmonella* pathogenicity island 1 (SPI-1) for epithelial cell invasion, genes from *Salmonella* pathogenicity island 2 (SPI-2) for intracellular replication, and flagellar genes for bacterial motility and colonization **(Figure 6e)**. We examined six representative targets: *hilD* and *sipA* (SPI-1), *ssaV* and *sifA* (SPI-2), and *flhDC* and *fliC* (flagellar regulation). Treatment with SKL significantly reduced the expression of all six genes by 50.0%-77% in the WT strain. In contrast, in the *ΔqseC* mutant, SKL had no effect on these gene expressions, and complementation with *qseC* fully restored SKL sensitivity **(Figure 6f–k)**. Furthermore, the expression of these six genes was dose‑dependently suppressed by SKL, with progressive reductions observed from ¼×MIC to 1×MIC **(Figure S9a–f)**. These results demonstrate that SKL acts through QseC to broadly suppress virulence gene expression, functionally attenuating the pathogen.

To test whether this anti-QseC mechanism contributes to antimicrobial activity *in vivo* and to further separate anti-virulence effect from direct bactericidal activity, we established a subinhibitory dose of SKL that has no direct bactericidal activity. At 5 mg/kg, SKL did not significantly reduce bacterial loads in the liver, spleen, or cecal contents compared to vehicle controls **(Figure S4b),** indicating minimal direct killing. Nevertheless, this dose of SKL improved mouse survival by 40%, whereas $(SKL)_4$ exhibited no protective efficacy **(Figure S10)**. To further confirm that SKL's *in vivo* protection relies on QseC suppression, we used the same subinhibitory SKL dose and performed a competitive infection experiment. Mice were co-infected with a 1:1 mixture of WT and *ΔqseC Salmonella* strains, followed by SKL or PBS treatment. We then determined the competitive index (CI) (CI= *ΔqseC* CFU / WT CFU) in the liver, spleen, ileum, cecal contents, and feces **(Figure 6l)**. In PBS-treated controls, CI was below 1 in the liver (~ 0.37), spleen (~ 0.40), and ileum (~ 0.43), confirming that the *ΔqseC* strain is less fit in these organs due to its virulence defect. In the cecal contents and feces, CIs were near or above 1 (~ 1.10), indicating active shedding of the *ΔqseC*

strain. Strikingly, SKL treatment raised the CI to near unity across all tissues (liver ~0.85, spleen ~0.89, ileum ~0.90, cecal contents ~1.02, feces ~1.05) **(Figure 6m)**. This shift demonstrates that SKL attenuates the WT strain's competitive advantage by inhibiting its QseC system, effectively phenocopying the *ΔqseC* mutant *in vivo*. Therefore, beyond any direct bactericidal activity, SKL provides a second layer of defense by disabling the QseC quorum-sensing circuit during infection.

Topical SKL and $(SKL)_4$ clear MRSA wound infections in mice

Given the growing clinical challenge due to multidrug-resistant pathogens such as methicillin-resistant *Staphylococcus aureus* (MRSA),[31] we next tested whether SKL and $(SKL)_4$ could treat localized wound infections by MRSA. We formulated SKL and $(SKL)_4$ into topical ointments and assessed their efficacy in a mouse model of MRSA-infected full-thickness skin wound **(Figure 7a)**. Mice received either SKL ointment, $(SKL)_4$ ointment, mupirocin (standard-of-care antibiotic),[32] or a vehicle control ointment. Wound closure was monitored on 3, 5, 7, 9, and 11 dpi. Both SKL and $(SKL)_4$ markedly accelerated wound healing compared to PBS vehicle, as shown by serial photographs **(Figure 7b)** and quantified by heatmap visualization of wound area dynamics **(Figure 7c)**. Healing rates were significantly higher in both SKL and $(SKL)_4$ treatment groups at all time points **(Figure 7d)**. By day 11, SKL treatment achieved 98.69% wound closure, which was no less than 98.17% observed with mupirocin, indicating potent therapeutic equivalence. Consistent with the improved healing, SKL and $(SKL)_4$ substantially reduced bacterial load in wound tissue. Both treatments with SKL and $(SKL)_4$ reduced MRSA CFU to 1.58% of vehicle control levels **(Figure 7e)**, comparable to mupirocin, highlighting their potential as alternative topical antimicrobial agents.

Discussion

The growing global burden of antimicrobial resistance (AMR) necessitates innovative strategies beyond conventional antibiotics.[1] The gut microbiome, shaped by long-term ecological selection, represents a natural reservoir of bioactive molecules whose peptide components often exhibit favorable host compatibility and stability *in vivo*.[33] In this study, we characterized a microbiome-derived tripeptide, SKL, secreted by a *Limosilactobacillus reuteri* P190 from the healthy piglet gut, which exhibits a distinct, concentration-dependent dual mechanism of action. At bactericidal concentration, SKL acts as a rapid membrane-disruptive agent; at sub-inhibitory regimes, it functions as an anti-virulence modulator by targeting the histidine kinase QseC. This bifunctional architecture of SKL introduces a programmable therapeutic framework: high-dose regimens can be deployed for acute, high-burden pathogen clearance, whereas low-dose interventions offer a precision-medicine approach to reduce pathogenesis while preserving the ecological integrity of the commensal microbiota.

Across a panel of 26 distinct *L. reuteri* isolates, we observed preferential activity against Gram-negative to Gram-positive pathogens. Our metabolomic and biochemical analyses revealed a high abundance of organic acids within the P190 supernatant, with neutralization assays confirming that acidification provides a critical physiological backdrop for inhibition. Concurrently with the well-established secretion of reuterin by this species,[34] our data support a model wherein *L. reuteri* P190 coordinates a multi-tiered antimicrobial offense: co-secreted organic acids lower the microenvironmental pH and destabilize target homeostasis, thereby acting as auxiliary agents that facilitate the primary, peptide-mediated membrane disruption. This cooperative secretome architecture highlights the clinical necessity of transitioning from single-metabolite isolation to ecological, multi-factorial screening paradigms during probiotic and postbiotic development.

A key advantage of SKL is its low propensity to induce resistance. Through 20 serial passages, neither the native peptide SKL nor its tandem repeats $(SKL)_4$ elicited any

detectable increase in MIC, contrasting sharply with the rapid resistance kinetics observed for the clinical counter-selections polymyxin B and vancomycin. This durability stems from fundamentally different mechanistic constraints. Pathogen resistance to polymyxin B typically involves discrete genetic adaptations. Specifically, PhoPQ/PmrAB-mediated lipid A remodeling or mcr-driven phosphoethanolamine transfer that neutralizes outer-membrane surface charge.[35-37] Similarly, vancomycin resistance relies on target site alterations or pronounced cell-wall thickening to sequester the drug.[38, 39] In contrast, the antibacterial activity of SKL is governed by a collective, biophysical interplay of its three residues: Lysine (K) drives electrostatic attraction to anionic outer bacterial membranes;[40, 41] leucine (L) mediates hydrophobic insertion to destabilize the bilayer core;[42, 43] and serine (S) fine-tunes overall amphiphilicity, promoting stable intramembrane aggregation and enhancing disruption of Gram-negative bacterial membranes.[44] By anchoring its bactericidal efficacy to global physical properties of the bacterial lipid bilayer rather than a single mutable protein receptor, SKL imposes a high evolutionary hurdle; pathogen escape would require macro-scale physiological remodeling of membrane composition, a trajectory typically accompanied by prohibitive biological fitness.[45]

The multi-valent engineering further highlights that the optimal peptide length is critical in peptide design. While tandem concatenation is a recognized tool to amplify peptide potency by increasing effective valency/avidity and promoting productive membrane engagement,[46, 47] excessive lengthening frequently introduces over-hydrophobicity, rendering candidates susceptible to self-aggregation[48] and reducing free bioavailability[49]. Our finding that extending the SKL motif to 6 or 9 severely compromised antimicrobial performance identifies $(SKL)_4$ as a highly optimized thermodynamic sweet spot. This tetramer successfully balances charge density, hydrophobic moment, and structural helicity, offering an engineering blueprint for calibrating the therapeutic index of short, ultra-small peptide scaffolds.

The QseC inhibitor, LED209, selectively blocks signal binding to QseC, preventing its autophosphorylation and thereby dampening QseC-dependent virulence gene expression without impacting growth dynamics. LED209 provided robust protection in

Salmonella models, although it did not influence *S.* typhimurium growth *in vitro*.[50] However, SKL integrates QseC-linked virulence suppression with direct membrane disruption and bactericidal activity. At subinhibitory concentrations, SKL downregulates *qseC* transcription and inhibits biofilm formation; while at bactericidal concentrations, it disrupts membranes and achieves complete killing. This dual-layer constraint effectively prevents QseC-dependent pathogen motility and invasion, which is conserved in many Gram-negative enteric pathogens,[26] while the membrane-lytic component handles strains lacking the target, such as MRSA. Consequently, the clinical spectrum of SKL is defined by a unique intersection of membrane vulnerability and signaling circuitry, making it uniquely suited for complex clinical indications where high bacterial burdens and aggressive virulence expression simultaneously drive host tissue damage.

Lastly, the striking disconnect observed between *in vitro* potency and *in vivo* efficacy reveals a nuanced pharmacokinetic reality. Despite $(SKL)_4$ demonstrating a 16-fold superior *in vitro* MIC against *S*. Typhimurium relative to monomeric SKL, both candidates yielded nearly indistinguishable survival benefits in systemic murine infection models. This lack of linear translation strongly points to complex physiological buffers, including differential proteolytic degradation, high serum-protein binding, or distinct tissue clearance rates that restrict the free-drug exposure of the larger tetramer at infected foci. Crucially, the sub-MIC anti-virulence activity unique to monomeric SKL is a therapeutic synergy completely masked by standard *in vitro* MIC assays. This positions SKL as a highly competitive clinical candidate. Their robust performance in MRSA-infected wound models, even matching the clinical standard mupirocin, highlights their potential as topical therapeutics for ischemic, hypoxic chronic wounds such as diabetic foot ulcers, where conventional antibiotic options are rapidly being exhausted.[51] Nevertheless, further work is required to evaluate the therapeutic potential of SKL and $(SKL)_4$ in these and additional clinically relevant models, as well as to define their long-term safety, the evolution of resistance under host-relevant conditions, and the molecular basis of the SKL-QseC interaction.

Conclusions

We demonstrate that *L. reuteri* P190, isolated from the piglet gut, exhibits strong antimicrobial activity both *in vitro* and *in vivo*. We further identified the tripeptide SKL as the primary effector molecule underpinning this antibacterial effect. Rational engineering into the tetravalent derivative $(SKL)_4$ improved charge distribution, conformational stability, and antibacterial potency while preserving host compatibility. Both SKL and $(SKL)_4$ act rapidly by disrupting bacterial membranes and confer robust protection against systemic and localized bacterial infections in murine models. Notably, at sub-inhibitory concentrations, SKL additionally attenuates virulence via suppression of QseC-dependent signaling, thereby impairing biofilm formation and pathogenicity. Collectively, this study unveils SKL as a novel antimicrobial peptide motif and underscores the value of ecological discovery and rational engineering for antimicrobial development.

Funding Statement

This work was supported by Zhejiang Province “San Nong Jiu Fang” Science and Technology Cooperation Program (2026SNJF040), the National Program on Key Research Project of China (2019YFE0103900), and Hangzhou Chengxi Sci-tech innovation Corridor Management Committee.

Acknowledgments

We thank Jiajia Wang and Yingying Huang from the Core Facilities, Zhejiang University School of Medicine for their technical supports. We also thank Yulan Jin, Xueqiu Chen, Weidong Zeng and Dandan Liu from the Experimental Teaching Center, College of Animal Sciences, Zhejiang University for using the qPCR instrument (LightCycler ® 480 II, Roche).

Declaration of Interest Statement

The other authors have no conflict of interest to declare

Data Availability Statement

The metabolomics data generated in this study have been deposited on Figshare (https://doi.org/10.6084/m9.figshare.32791506). All other data supporting the findings of this study are available from the corresponding author upon reasonable request.

Author contributions

Y L, Q L, M Y and BK W provide experimental ideas and design the study. Q L, D W, HJ J, HJ W, N L, LH Y, YF F, LY M and K Z conducted the experiments. Q L and HJ W analyzed and interpreted the data. Q L and Y L drafted the manuscript. Y L reviewed and edited the manuscript.

References

1. Collaborators GAR. Global burden of bacterial antimicrobial resistance 1990-2021: a systematic analysis with forecasts to 2050. Lancet (London, England) 2024; 404:1199-226.
2. Sati H, Carrara E, Savoldi A, Hansen P, Garlasco J, Campagnaro E, et al. The WHO Bacterial Priority Pathogens List 2024: a prioritisation study to guide research, development, and public health strategies against antimicrobial resistance. The Lancet Infectious diseases 2025; 25:1033-43.
3. Oliveira Júnior NG, Souza CM, Buccini DF, Cardoso MH, Franco OL. Antimicrobial peptides: structure, functions and translational applications. Nature reviews Microbiology 2025; 23:687-700.
4. Wang Y, Zhao L, Li Z, Xi Y, Pan Y, Zhao G, et al. A generative artificial intelligence approach for the discovery of antimicrobial peptides against multidrug-resistant bacteria. Nature microbiology 2025; 10:2997-3012.
5. Chen EH, Wang CH, Liao YT, Chan FY, Kanaoka Y, Uchihashi T, et al. Visualizing the membrane disruption action of antimicrobial peptides by cryo-electron tomography. Nature communications 2023; 14:5464.
6. Bhaumik KN, Spohn R, Dunai A, Daruka L, Olajos G, Zákány F, et al. Chemically diverse antimicrobial peptides induce hyperpolarization of the E. coli membrane. Communications biology 2024; 7:1264.
7. Tajer L, Paillart JC, Dib H, Sabatier JM, Fajloun Z, Abi Khattar Z. Molecular Mechanisms of Bacterial Resistance to Antimicrobial Peptides in the Modern Era: An Updated Review. Microorganisms 2024; 12:1259.
8. Wang Y, Shi YN, Xiang H, Shi YM. Exploring nature's battlefield: organismic interactions in the discovery of bioactive natural products. Natural product reports 2024; 41:1630-51.
9. Hussain A, Patwekar U, Mongad DS, Shouche YS. Strategizing the human microbiome for small molecules: Approaches and perspectives. Drug discovery today 2023; 28:103459.
10. Santos-Júnior CD, Torres MDT, Duan Y, Rodríguez Del Río Á, Schmidt TSB, Chong H, et al. Discovery of antimicrobial peptides in the global microbiome with machine learning. Cell 2024; 187:3761-78.e16.
11. Ma Y, Guo Z, Xia B, Zhang Y, Liu X, Yu Y, et al. Identification of antimicrobial peptides from the human gut microbiome using deep learning. Nature biotechnology 2022; 40:921-31.
12. Du R, Han F, Li Z, Yu J, Xu Y, Huang Y, et al. Uncovering encrypted antimicrobial peptides in health-associated Lactobacillaceae by large-scale genomics and machine learning. Microbiome 2025; 13:151.
13. Javadi H, Lehnen AC, Hartlieb M. Bioinspired Cationic Antimicrobial Polymers. Angewandte Chemie (International ed in English) 2025; 64:e202503738.
14. Castillo-Juárez I, Blancas-Luciano BE, García-Contreras R, Fernández-Presas AM. Antimicrobial peptides properties beyond growth inhibition and bacterial killing. PeerJ 2022; 10:e12667.
15. Daher R, Pouget C, Lavigne JP, François P, Dunyach-Remy C. Anti-virulence peptides: a compromising strategy to treat Staphylococcus aureus chronic wound infection. Critical reviews in microbiology 2026; 52:414-32.
16. Hairsine B, Leire E, Rostam HM, Kristian SA, Rhodes E, Johnson A, et al. Harnessing endogenous anti-glycan antibodies using a novel, bifunctional immunotherapy to treat gram-negative bacterial infections. Journal of immunology (Baltimore, Md : 1950) 2025; 214:1617-29.
17. Gorzelanna Z, Mamrot A, Będkowska D, Bubak J, Miszczak M. Exploring the Potential of Novel Animal-Origin Probiotics as Key Players in One Health: Opportunities and Challenges. International

603 journal of molecular sciences 2025; 26:5143.
604 18. Teng K, Huang F, Liu Y, Wang Y, Xia T, Yun F, et al. Food and gut originated bacteriocins involved
605 in gut microbe-host interactions. Critical reviews in microbiology 2023; 49:515-27.
606 19. Jones RN, Anderegg TR, Swenson JM. Quality control guidelines for testing gram-negative control
607 strains with polymyxin B and colistin (polymyxin E) by standardized methods. Journal of clinical
608 microbiology 2005; 43:925-7.
609 20. Brango-Vanegas J, Leite ML, Macedo MLR, Cardoso MH, Franco OL. Capping motifs in
610 antimicrobial peptides and their relevance for improved biological activities. Frontiers in chemistry 2024;
611 12:1382954.
612 21. Zhong C, Zhang F, Yao J, Zhu Y, Zhu N, Zhang J, et al. New Antimicrobial Peptides with Repeating
613 Unit against Multidrug-Resistant Bacteria. ACS infectious diseases 2021; 7:1619-37.
614 22. Zhong C, He Y, Zou J, Gao L, Wang J, Zhu J, et al. An antimicrobial peptide as a potential therapy
615 for bacterial pneumonia that alleviates antimicrobial resistance. Nature communications 2025;
616 16:10488.
617 23. Guha S, Ghimire J, Wu E, Wimley WC. Mechanistic Landscape of Membrane-Permeabilizing
618 Peptides. Chemical reviews 2019; 119:6040-85.
619 24. Domouchtsidou A, Ioannou P, Lianou A, Tsante KA, Tsakri D, Bonova E, et al. Biofilms in clinical
620 infection: pathophysiology, diagnosis, and the evolving therapeutic landscape. Journal of clinical
621 microbiology 2025; 64:e0104225.
622 25. Yan C, Li X, Zhang G, Bi J, Hao H, Hou H. The Regulatory Role of Quorum Sensing-Mediated
623 Amino Acid Metabolism in Biofilm Formation and Motility of Hafnia alvei H4. Foods (Basel, Switzerland)
624 2026; 15:281.
625 26. Zhu Y, Dou Q, Du L, Wang Y. QseB/QseC: a two-component system globally regulating bacterial
626 behaviors. Trends in microbiology 2023; 31:749-62.
627 27. Bader MW, Sanowar S, Daley ME, Schneider AR, Cho U, Xu W, et al. Recognition of antimicrobial
628 peptides by a bacterial sensor kinase. Cell 2005; 122:461-72.
629 28. Yang H, Jiang X, Nychas GE, Yang K, Dong P, Zhang Y, et al. Role of the PhoP/PhoQ Two-
630 Component Regulatory System in Biofilm Formation in Acid-Adapted Salmonella typhimurium. Foods
631 (Basel, Switzerland) 2025; 14:4344.
632 29. Schachterle JK, Sundin GW. The Leucine-Responsive Regulatory Protein Lrp Participates in
633 Virulence Regulation Downstream of Small RNA ArcZ in Erwinia amylovora. mBio 2019; 10:e00757-19.
634 30. Li D, Shi Q, He L, Luo J, Zhu H, Hua X, et al. Cpx-mediated amino acid sensing diversifies
635 gastrointestinal colonization of Klebsiella pneumoniae. mLife 2025; 4:181-92.
636 31. Parsons JB, Mourad A, Conlon BP, Kielian T, Fowler VG, Jr. Methicillin-resistant and susceptible
637 Staphylococcus aureus: tolerance, immune evasion and treatment. Nature reviews Microbiology 2026;
638 24:127-45.
639 32. Septimus EJ, Schweizer ML. Decolonization in Prevention of Health Care-Associated Infections.
640 Clinical microbiology reviews 2016; 29:201-22.
641 33. Torres MDT, Brooks EF, Cesaro A, Sberro H, Gill MO, Nicolaou C, et al. Mining human microbiomes
642 reveals an untapped source of peptide antibiotics. Cell 2024; 187:5453-67.e15.
643 34. Ortiz-Rivera Y, Sánchez-Vega R, Gutiérrez-Méndez N, León-Félix J, Acosta-Muñiz C, Sepulveda
644 DR. Production of reuterin in a fermented milk product by Lactobacillus reuteri: Inhibition of pathogens,
645 spoilage microorganisms, and lactic acid bacteria. Journal of dairy science 2017; 100:4258-68.
646 35. Huang J, Li C, Song J, Velkov T, Wang L, Zhu Y, et al. Regulating polymyxin resistance in Gram-

negative bacteria: roles of two-component systems PhoPQ and PmrAB. Future microbiology 2020; 15:445-59.
36. Liu YY, Wang Y, Walsh TR, Yi LX, Zhang R, Spencer J, et al. Emergence of plasmid-mediated colistin resistance mechanism MCR-1 in animals and human beings in China: a microbiological and molecular biological study. The Lancet Infectious diseases 2016; 16:161-8.
37. Gao R, Hu Y, Li Z, Sun J, Wang Q, Lin J, et al. Dissemination and Mechanism for the MCR-1 Colistin Resistance. PLoS pathogens 2016; 12:e1005957.
38. Reynolds PE, Courvalin P. Vancomycin resistance in enterococci due to synthesis of precursors terminating in D-alanyl-D-serine. Antimicrobial agents and chemotherapy 2005; 49:21-5.
39. Rose WE, Knier RM, Hutson PR. Pharmacodynamic effect of clinical vancomycin exposures on cell wall thickness in heterogeneous vancomycin-intermediate Staphylococcus aureus. The Journal of antimicrobial chemotherapy 2010; 65:2149-54.
40. Kumar P, Kizhakkedathu JN, Straus SK. Antimicrobial Peptides: Diversity, Mechanism of Action and Strategies to Improve the Activity and Biocompatibility In Vivo. Biomolecules 2018; 8:4.
41. Wang J, Zeng F, Chen X, Wang T, Wang L, Zhou M, et al. Engineering of antimicrobial peptide Brevinin-1pl: arginine, lysine, and histidine substitutions enhance antimicrobial-anticancer efficacy with reduced cytotoxicity. Frontiers in chemistry 2025; 13:1579097.
42. Lobka M, Siekierska I, Chyży P, Burmistrz M, Macyszyn J, Grzela R, et al. Design, synthesis and evaluation of lysine- and leucine-rich hydrocarbon-stapled peptides as antibacterial agents. European journal of medicinal chemistry 2025; 290:117445.
43. Chen Y, Guarnieri MT, Vasil AI, Vasil ML, Mant CT, Hodges RS. Role of peptide hydrophobicity in the mechanism of action of alpha-helical antimicrobial peptides. Antimicrobial agents and chemotherapy 2007; 51:1398-406.
44. Stephens A, Ge T, Ding K, Hollowell P, Clifton L, Hall S, et al. Selective Serine Substitutions of Antimicrobial Peptides Reveal Different Mechanistic Actions Toward Gram-Negative Bacteria. ACS applied materials & interfaces 2026; 18:10860-73.
45. Spohn R, Daruka L, Lázár V, Martins A, Vidovics F, Grézal G, et al. Integrated evolutionary analysis reveals antimicrobial peptides with limited resistance. Nature communications 2019; 10:4538.
46. Liu SP, Zhou L, Lakshminarayanan R, Beuerman RW. Multivalent Antimicrobial Peptides as Therapeutics: Design Principles and Structural Diversities. International journal of peptide research and therapeutics 2010; 16:199-213.
47. Pratap Verma D, Ansari MM, Verma NK, Saroj J, Akhtar S, Pant G, et al. Tandem Repeat of a Short Human Chemerin-Derived Peptide and Its Nontoxic d-Lysine-Containing Enantiomer Display Broad-Spectrum Antimicrobial and Antitubercular Activities. Journal of medicinal chemistry 2021; 64:15349-66.
48. Thapa S, Gahlawat A, Schneebeli ST, Li J. Interplay of Hydrophobicity, Charge, and Sequence Length in Oligopeptide Coassembly. The Journal of Physical Chemistry B 2025; 129:4383-91.
49. Acquah C, Di Stefano E, Udenigwe CC. Role of hydrophobicity in food peptide functionality and bioactivity. Journal of Food Bioactives 2018; 4:88-98.
50. Rasko DA, Moreira CG, Li de R, Reading NC, Ritchie JM, Waldor MK, et al. Targeting QseC signaling and virulence for antibiotic development. Science (New York, NY) 2008; 321:1078-80.
51. Tarigan MB, Saragih RM, Tarigan KA, Ginting F. Antimicrobial resistance and empirical antibiotic use in diabetic foot infections: A retrospective study from Indonesia. Narra J 2025; 5:e2895.

FIGURE LEGENDS

Figure 1. Gut-derived *Limosilactobacillus reuteri* P190 exhibits broad-spectrum antibacterial activity and confers protection against systemic *Salmonella* Typhimurium SL1344 infection in C57BL/6 mice.

(a) Schematic of the sequential isolation and screening workflow from piglet intestinal contents, showing the number and proportion of isolates at each step and the ultimate identification of *L. reuteri* P190.

(b) Heatmap depicting the antimicrobial activity of 26 isolated *L. reuteri* strains against a panel of clinically relevant pathogens. Inhibition zone diameters (mm) are represented by a color gradient.

(c) Schematic of experimental timeline for the murine model of systemic *S.* Typhimurium SL1344 infection.

(d, e) Body weight changes (d) and survival rates (e) of mice following *S.* Typhimurium SL1344 infection (n = 10 per group).

(f) Bacterial loads (CFU) in the liver, spleen, cecal contents, and blood at 3 days post-infection (dpi) (n = 6 per group). The dashed line indicates the limit of detection (LOD).

(g, h) Histological examination of H&E-stained liver (g) and spleen (h) sections. Mock group (uninfected, untreated) served as the healthy control. PBS-STM and P190-STM groups were infected with *S*. Typhimurium SL1344 and received sterile PBS or *L. reuteri* P190, respectively.

Data are shown as the mean ± SD. Statistical significance for body weight changes and bacteria loads was determined using two-way ANOVA, whereas survival curves were analyzed using the log-rank (Mantel-Cox) test. * $p < 0.05$; ** $p < 0.01$; *** $p < 0.001$; ns, not significant.

Figure 2. Identification of the secreted tripeptide SKL as the key antimicrobial effector of *Limosilactobacillus reuteri* P190.

(a) Antimicrobial activity of *L. reuteri* P190 whole culture (P190), cell-free

supernatant (P190 sup), and washed cell pellet (P190 pel) against *S.* Typhimurium SL1344, assessed by agar well diffusion assay. The dashed line indicates the threshold for detectable activity.

(b) Growth inhibition of *S.* Typhimurium SL1344 by MRS medium, untreated P190 cell-free supernatant (P190 sup), and P190 cell-free supernatant digested with pepsin (P190 sup-pepsin) or trypsin (P190 sup-trypsin), monitored by OD_{600} over 24 hours.

(c) Inhibition zone diameters of untreated P190 cell-free supernatant (Untreated) and P190 cell-free supernatant digested with pepsin or trypsin against *S.* Typhimurium SL1344, determined by agar well diffusion assay.

(d) Schematic of experimental timeline for the murine model of systemic *S.* Typhimurium SL1344 infection.

(e, f) Body weight changes (e) and survival rates (f) of mice following *S.* Typhimurium SL1344 infection (n = 10 per group).

(g) Bacterial loads (CFU) in the liver, spleen, cecal contents, and blood at 3 dpi (n = 6 per group). The dashed line indicates the limit of detection (LOD).

(h) Principal component analysis (PCA) score plot of untargeted metabolomics data from *L. reuteri* P190 and P126 cell-free supernatants. Ellipses represent the 95% confidence intervals (n = 6 per group).

(i) Abundance ranking of differently expressed metabolites (DEM) identified between P190 and P126 supernatants.

(j) Volcano plot of DEMs, highlighting metabolites significantly upregulated in P190 (log_2-fold change > 1, $p < 0.05$).

(k) Chemical structure of the tripeptide SKL (Ser-Lys-Leu) from PubChem.

(l) *In silico* prediction of trypsin and pepsin cleavage sites within the SKL sequence.

(m) Minimum inhibitory concentrations (MIC) of SKL against *S.* Typhimurium SL1344, determined with or without prior digestion by pepsin or trypsin.

Data are shown as the mean ± SD. Statistical significance of body weight changes and growth curves was assessed using one-way ANOVA or two-way ANOVA; survival curves were compared using the log-rank (Mantel-Cox) test. * $p < 0.05$; ** $p < 0.01$; *** $p < 0.001$; ns, not significant.

Figure 3. Tandem-repeat optimization of SKL enhances antimicrobial activity and establishes $(SKL)_4$ as the lead candidate.

(a) AlphaFold-predicted secondary structures of SKL tandem-repeat peptides $(SKL)_3$ through $(SKL)_9$.

(b) Bubble plot depicting the minimum inhibitory concentrations (MIC, μg/mL) of SKL and its tandem-repeat peptides against a panel of bacterial strains indicated in the figure. MIC values are encoded by both color intensity and bubble size, as defined in the scale.

(c) Hemolytic activity and viability of RAW264.7 cells following treatment with SKL and its tandem-repeat peptides.

(d) Time-kill kinetics of SKL and $(SKL)_4$ against *S.* Typhimurium SL1344 at 1×MIC and 1× minimum bactericidal concentration (MBC).

(e, f) Development of resistance in *S.* Typhimurium SL1344(e) and in methicillin-resistant *S. aureus* (MRSA) (f) under ½ x MIC concentrations of SKL, $(SKL)_4$, polymyxin B, or vancomycin.

Data are shown as the mean ± SD. Statistical significance was assessed using one-way ANOVA. * $p < 0.05$; ** $p < 0.01$; *** $p < 0.001$; ns, not significant.

Figure 4. SKL and $(SKL)_4$ exert bactericidal activity through disrupting membrane integrity.

(a) Scanning electron microscopy (SEM) micrographs of *Salmonella* Typhimurium SL1344 and methicillin-resistant *Staphylococcus aureus* (MRSA) cells treated with SKL or $(SKL)_4$ at 1×MIC for 1 h. PBS-treated cells served as the vehicle control.

(b) Outer membrane permeability of *S.* Typhimurium SL1344 following treatment with PBS vehicle, SKL, or $(SKL)_4$, measured via NPN fluorescence uptake assay.

(c) Inner membrane permeability of *S.* Typhimurium SL1344 treated with PBS vehicle, SKL, or $(SKL)_4$, indicated by the hydrolysis of ONPG and monitored by OD_{420}.

(d, e) Leakage of cellular contents from *S.* Typhimurium SL1344 after treatment with SKL or $(SKL)_4$ at 1×MIC for the indicated durations, determined by absorbance at

OD_{260} for nucleic acid (d) and OD_{280} for protein (e). PBS-treated cells were served as vehicle control.

(f) Membrane fluidity of *S.* Typhimurium SL1344 treated with PBS vehicle, SKL, or $(SKL)_4$, assessed by DPH fluorescence polarization assay.

(g) Membrane hydrophobicity of *S.* Typhimurium SL1344 treated with PBS vehicle, SKL, or $(SKL)_4$, assessed by hexadecane partitioning assay.

Data are shown as the mean ± SD. Statistical significance was assessed by one-way ANOVA. * $p < 0.05$; ** $p < 0.01$; *** $p < 0.001$; ns, not significant.

Figure 5. SKL and $(SKL)_4$ confer protection against systemic *Salmonella* infection in immunocompromised neutropenic mice.

(a) Schematic of experimental timeline for the cyclophosphamide-induced neutropenic murine model of systemic *S.* Typhimurium SL1344 infection.

(b, c) Body weight changes (b) and survival rates (c) of mice following *S.* Typhimurium SL1344 infection (n = 10 per group).

(d) Bacterial loads (CFU) in the liver, spleen, cecal contents, and blood at 2 dpi (n = 6 per group). The dashed line indicates the limit of detection (LOD).

Data are shown as the mean ± SD. Statistical significance for body weight changes and bacterial loads was assessed using two-way ANOVA; survival curves were analyzed using the log-rank (Mantel-Cox) test. * $p < 0.05$; ** $p < 0.01$; *** $p < 0.001$; ns, not significant.

Figure 6. SKL targets the QseC histidine kinase to suppress *Salmonella* virulence and pathogenicity.

(a) Inhibition of *S.* Typhimurium SL1344 biofilm formation by SKL and $(SKL)_4$ at the indicated concentrations (¼×, ½×, 1× MIC). PBS served as the vehicle control, and polymyxin B at 4×MIC was used as a positive control.

(b) Quantitative real-time PCR (qRT-PCR) analysis of *qseC*, *phoP*, *lrp*, and *cpxA* mRNA levels in *S.* Typhimurium SL1344 treated with PBS vehicle or SKL or $(SKL)_4$.

(c) qRT-PCR analysis of *qseC* mRNA levels in *S.* Typhimurium SL1344 following

809 treatment with vehicle or increasing concentrations of SKL (¼×, ½×, and1×MIC).

810 (d) Western blot analysis of QseC and RpoB (loading control) protein levels in wild-
811 type (WT), *ΔqseC* (*qseC* knockout), and complemented (C-*ΔqseC*) *S.* Typhimurium
812 strains, with (+) or without (-) SKL treatment (upper panel). Densitometric quantification
813 of QseC protein levels relative to RpoB, normalized to the WT vehicle group (lower
814 panel).

815 (e) Schematic of the QseB/QseC two-component system regulon in *S.* Typhimurium
816 1344, depicting the regulation of *Salmonella* pathogenicity island 1 (SPI-1) genes (*hilD*,
817 *sipA*) for epithelial invasion, SPI-2 genes (*ssaV*, *sifA*) for intracellular replication, and
818 flagellar genes (*flhDC*, *fliC*) for motility and colonization.

819 (f-k) qRT-PCR analysis of *hilD* (f), *sipA* (g), *ssaV* (h), *sifA* (i), *flhDC* (j), and *fliC* (k)
820 mRNA levels in WT, *ΔqseC*, and C-*ΔqseC S. Typhimurium* strains treated with PBS
821 vehicle or SKL at a subinhibitory concentration (¼×MIC).

822 (l) Experimental scheme for competitive infection assay in mice.

823 (m) Competitive index in the indicated tissues from vehicle- and SKL-treated mice
824 (n = 6 per group).

825 Data are shown as the mean ± SD. Statistical significance was assessed by two-
826 way ANOVA. * $p < 0.05$; ** $p < 0.01$; *** $p < 0.001$; ns, not significant.

827

828 **Figure 7. SKL and $(SKL)_4$ ointment exhibit potent therapeutic efficacy in a mouse**
829 **model of methicillin-resistant *Staphylococcus aureus* (MRSA) wound infection.**

830 (a) Schematic of experimental timeline of MRSA wound infection in mice.

831 (b) Representative photographs of wounds in MRSA-infected mice on 3, 5, 7, 9,
832 and 11 dpi following the indicated treatment.

833 (c) Wound closure kinetics in MRSA-infected mice over the treatment course.

834 (d) Percentage of wound healing at each indicated time point (n = 6 per group).

835 (e) Residual MRSA burden (CFU) in wound tissues after various treatments (n = 6
836 per group). The dashed line indicates the limit of detection (LOD).

837 Data are shown as the mean ± SD. Statistical significance was determined by one-
838 way ANOVA or two-way ANOVA. * $p < 0.05$; ** $p < 0.01$; *** $p < 0.001$; ns, not significant.

Fig 1

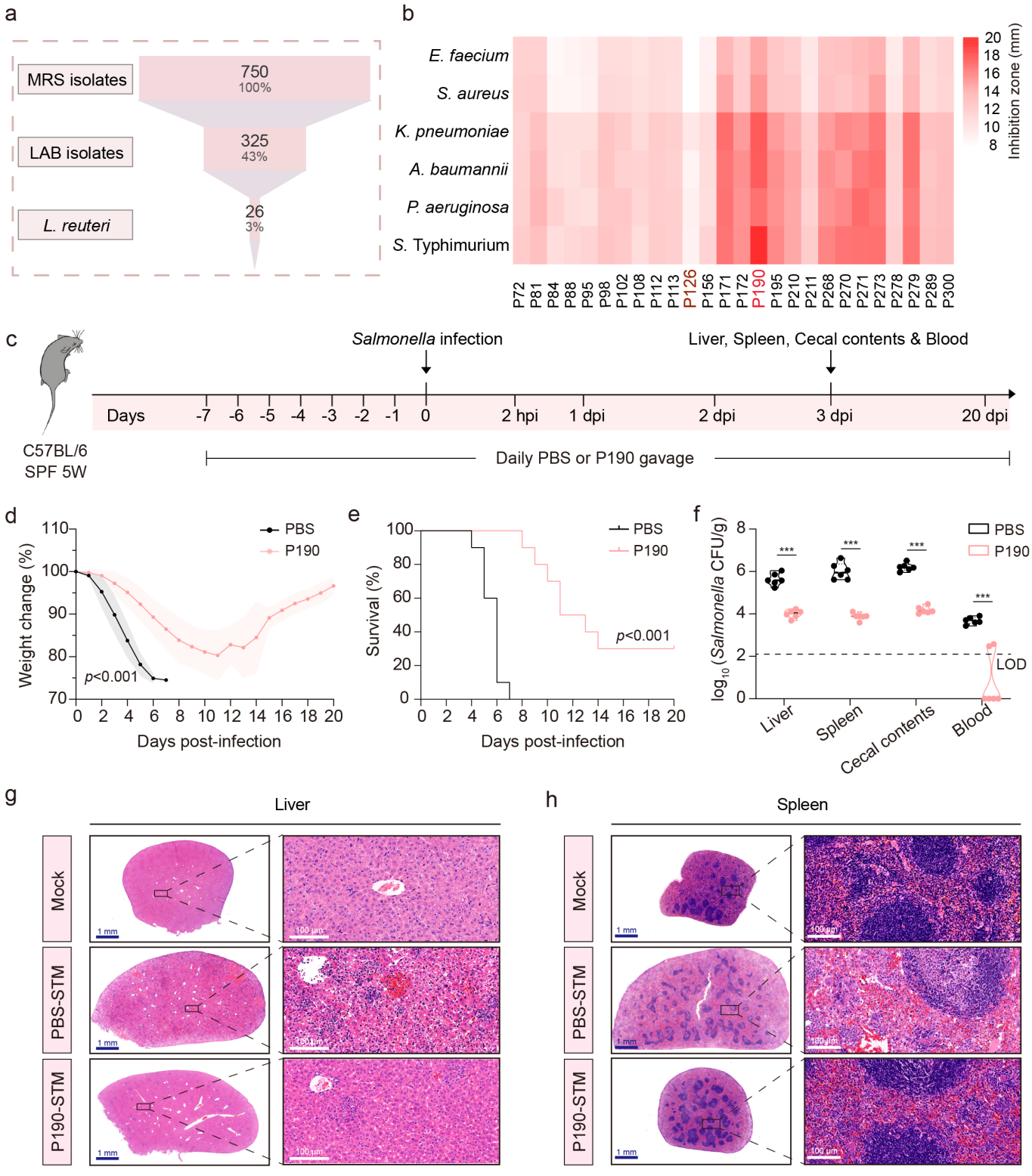
a
MRS isolates
750
100%
LAB isolates
325
43%
L. reuteri
26
3%
b
E. faecium
S. aureus
K. pneumoniae
A. baumannii
P. aeruginosa
S. Typhimurium
Inhibition zone (mm)
20
18
16
14
12
10
8
P72 P81 P84 P88 P95 P98 P102 P108 P112 P113 P126 P156 P171 P172 P190 P195 P210 P211 P268 P270 P271 P273 P278 P279 P289 P300
c
C57BL/6
SPF 5W
Salmonella infection
Liver, Spleen, Cecal contents & Blood
Days -7 -6 -5 -4 -3 -2 -1 0 2 hpi 1 dpi 2 dpi 3 dpi 20 dpi
Daily PBS or P190 gavage
d
Weight change (%)
PBS
P190
p<0.001
Days post-infection
e
Survival (%)
PBS
P190
p<0.001
Days post-infection
f
log10 (Salmonella CFU/g)
PBS
P190
***
LOD
Liver
Spleen
Cecal contents
Blood
g
Liver
Mock
PBS-STM
P190-STM
1 mm
100 μm
h
Spleen
Mock
PBS-STM
P190-STM
1 mm
100 μm

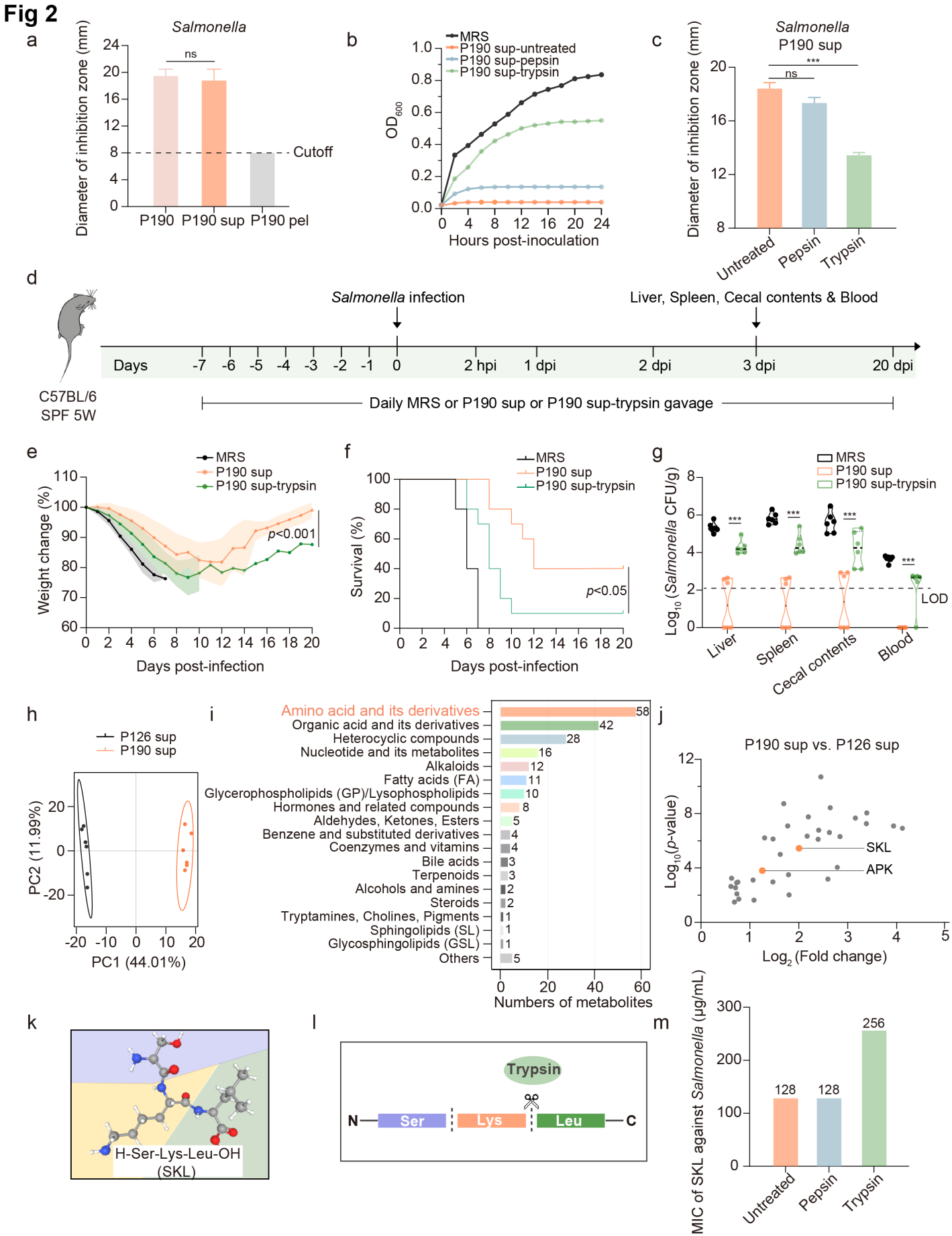
Fig 2
a
Salmonella
Diameter of inhibition zone (mm)
ns
Cutoff
P190
P190 sup
P190 pel
b
MRS
P190 sup-untreated
P190 sup-pepsin
P190 sup-trypsin
OD600
Hours post-inoculation
c
Salmonella
P190 sup
Diameter of inhibition zone (mm)
***
ns
Untreated
Pepsin
Trypsin
d
Salmonella infection
Liver, Spleen, Cecal contents & Blood
Days
-7 -6 -5 -4 -3 -2 -1 0
2 hpi
1 dpi
2 dpi
3 dpi
20 dpi
C57BL/6
SPF 5W
Daily MRS or P190 sup or P190 sup-trypsin gavage
e
MRS
P190 sup
P190 sup-trypsin
Weight change (%)
p<0.001
Days post-infection
f
MRS
P190 sup
P190 sup-trypsin
Survival (%)
p<0.05
Days post-infection
g
MRS
P190 sup
P190 sup-trypsin
Log10 (Salmonella CFU/g)
***
LOD
Liver
Spleen
Cecal contents
Blood
h
P126 sup
P190 sup
PC2 (11.99%)
PC1 (44.01%)
i
Amino acid and its derivatives 58
Organic acid and its derivatives 42
Heterocyclic compounds 28
Nucleotide and its metabolites 16
Alkaloids 12
Fatty acids (FA) 11
Glycerophospholipids (GP)/Lysophospholipids 10
Hormones and related compounds 8
Aldehydes, Ketones, Esters 5
Benzene and substituted derivatives 4
Coenzymes and vitamins 4
Bile acids 3
Terpenoids 3
Alcohols and amines 2
Steroids 2
Tryptamines, Cholines, Pigments 1
Sphingolipids (SL) 1
Glycosphingolipids (GSL) 1
Others 5
Numbers of metabolites
j
P190 sup vs. P126 sup
Log10(p-value)
SKL
APK
Log2 (Fold change)
k
H-Ser-Lys-Leu-OH
(SKL)
l
Trypsin
N
Ser
Lys
Leu
C
m
MIC of SKL against Salmonella (μg/mL)
256
128
128
Untreated
Pepsin
Trypsin

Fig 3

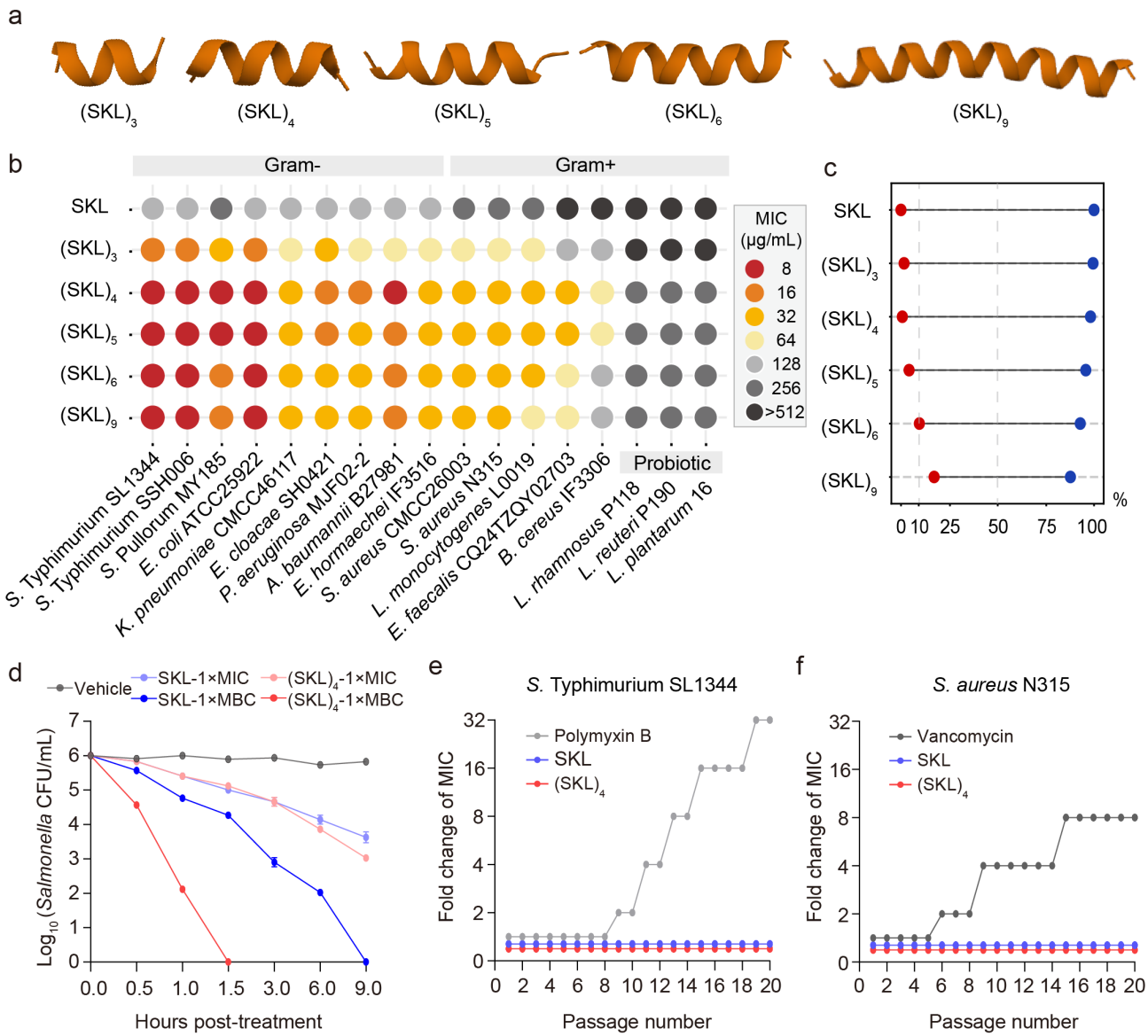
a
(SKL)3
(SKL)4
(SKL)5
(SKL)6
(SKL)9
b
Gram-
Gram+
SKL
(SKL)3
(SKL)4
(SKL)5
(SKL)6
(SKL)9
MIC (μg/mL)
8
16
32
64
128
256
>512
S. Typhimurium SL1344
S. Typhimurium SSH006
S. Pullorum MY185
E. coli ATCC25922
K. pneumoniae CMCC46117
E. cloacae SH0421
P. aeruginosa MJF02-2
A. baumannii B27981
E. hormaechei IF3516
S. aureus CMCC26003
S. aureus N315
L. monocytogenes L0019
E. faecalis CQ24TZQY02703
B. cereus IF3306
Probiotic
L. rhamnosus P118
L. reuteri P190
L. plantarum 16
c
SKL
(SKL)3
(SKL)4
(SKL)5
(SKL)6
(SKL)9
0 10 25 50 75 100
%
d
Vehicle
SKL-1×MIC
(SKL)4-1×MIC
SKL-1×MBC
(SKL)4-1×MBC
Log10 (Salmonella CFU/mL)
0 1 2 3 4 5 6 7
0.0 0.5 1.0 1.5 3.0 6.0 9.0
Hours post-treatment
e
S. Typhimurium SL1344
Polymyxin B
SKL
(SKL)4
Fold change of MIC
0 2 4 8 16 32
0 2 4 6 8 10 12 14 16 18 20
Passage number
f
S. aureus N315
Vancomycin
SKL
(SKL)4
Fold change of MIC
0 2 4 8 16 32
0 2 4 6 8 10 12 14 16 18 20
Passage number

Fig 4

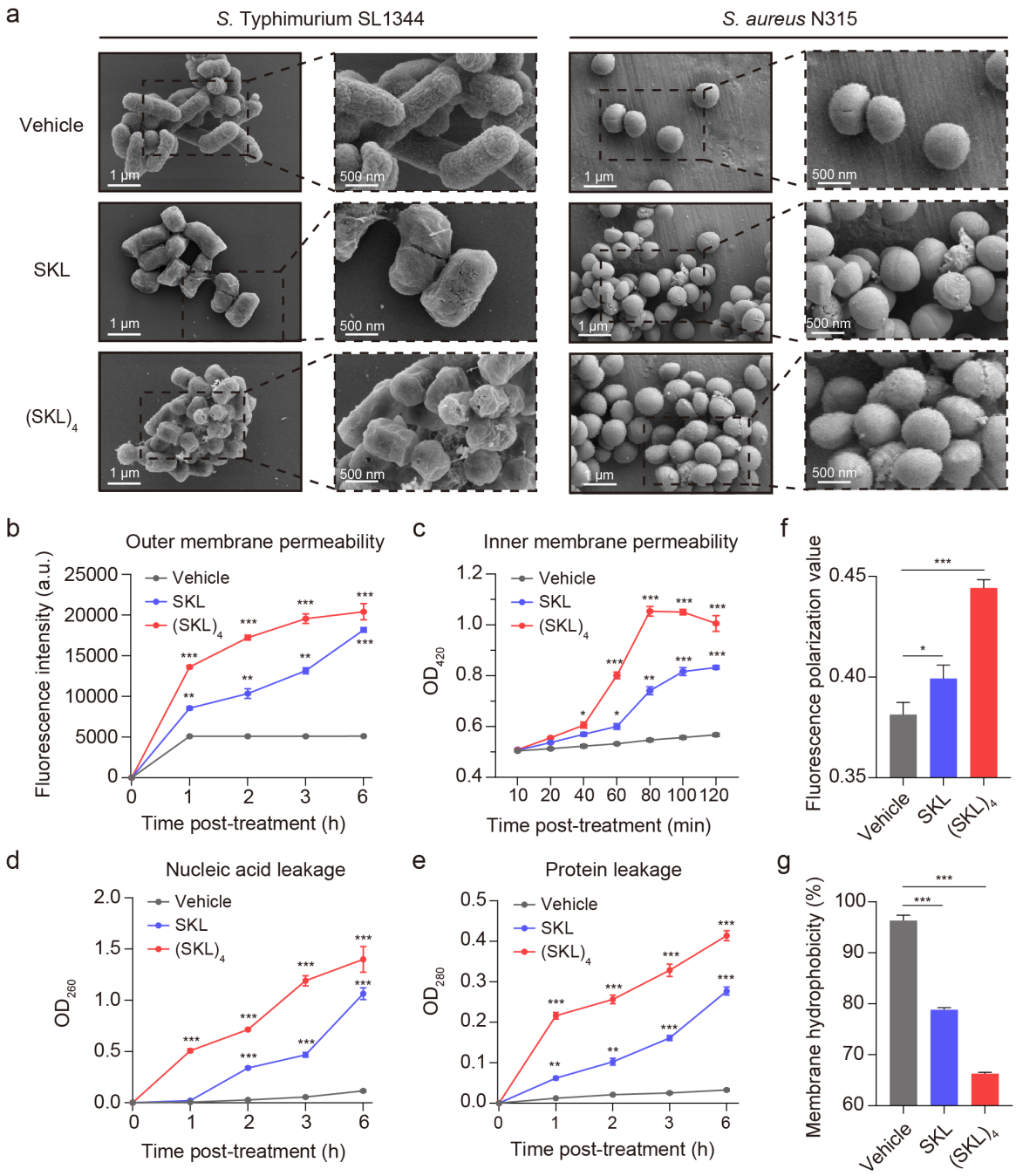
a
S. Typhimurium SL1344
S. aureus N315
Vehicle
SKL
(SKL)4
1 μm
500 nm
b
Outer membrane permeability
Fluorescence intensity (a.u.)
Time post-treatment (h)
c
Inner membrane permeability
OD420
Time post-treatment (min)
f
Fluorescence polarization value
d
Nucleic acid leakage
OD260
e
Protein leakage
OD280
g
Membrane hydrophobicity (%)
Vehicle
SKL
(SKL)4

Fig 5

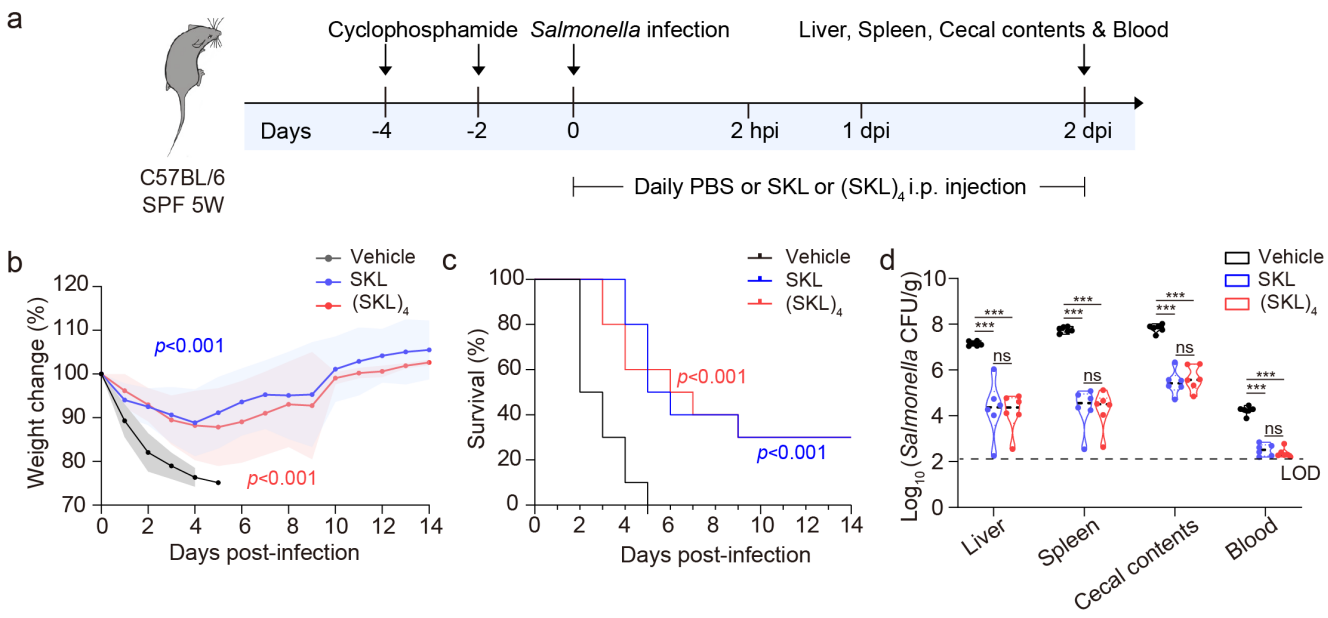
a
Cyclophosphamide
Salmonella infection
Liver, Spleen, Cecal contents & Blood
Days
-4
-2
0
2 hpi
1 dpi
2 dpi
C57BL/6
SPF 5W
Daily PBS or SKL or (SKL)4 i.p. injection
b
Vehicle
SKL
(SKL)4
Weight change (%)
p<0.001
p<0.001
Days post-infection
c
Survival (%)
p<0.001
p<0.001
Days post-infection
d
Log10 (Salmonella CFU/g)
***
ns
LOD
Liver
Spleen
Cecal contents
Blood

Fig 6

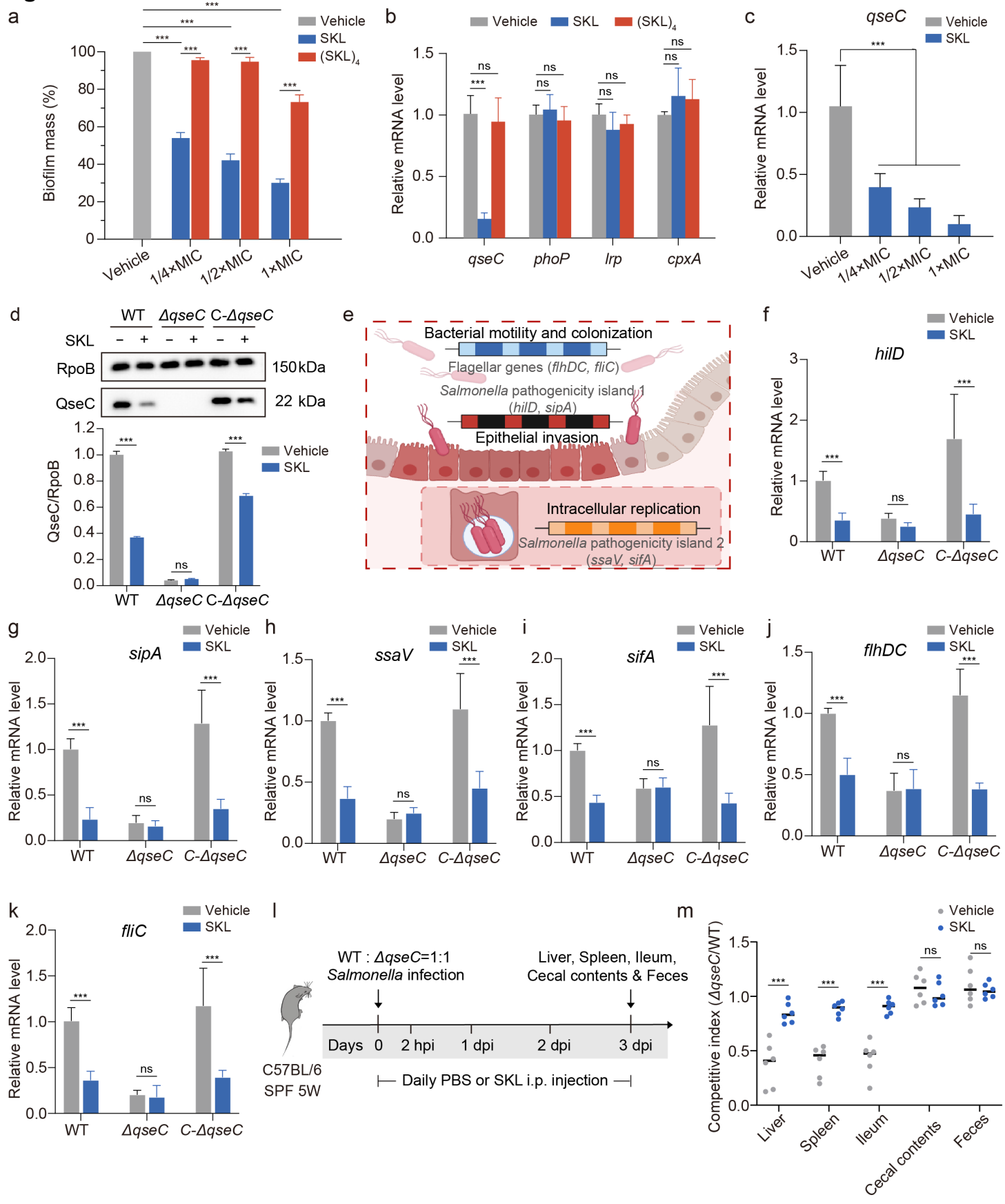
a
Vehicle
SKL
(SKL)4
Biofilm mass (%)
Vehicle
1/4×MIC
1/2×MIC
1×MIC
b
Vehicle
SKL
(SKL)4
Relative mRNA level
qseC
phoP
lrp
cpxA
c
qseC
Vehicle
SKL
Relative mRNA level
Vehicle
1/4×MIC
1/2×MIC
1×MIC
d
WT
ΔqseC
C-ΔqseC
SKL
RpoB
150kDa
QseC
22 kDa
QseC/RpoB
Vehicle
SKL
WT
ΔqseC
C-ΔqseC
e
Bacterial motility and colonization
Flagellar genes (flhDC, fliC)
Salmonella pathogenicity island 1
(hilD, sipA)
Epithelial invasion
Intracellular replication
Salmonella pathogenicity island 2
(ssaV, sifA)
f
hilD
Vehicle
SKL
Relative mRNA level
WT
ΔqseC
C-ΔqseC
g
sipA
h
ssaV
i
sifA
j
flhDC
k
fliC
l
WT : ΔqseC=1:1
Salmonella infection
Liver, Spleen, Ileum,
Cecal contents & Feces
Days 0 2 hpi 1 dpi 2 dpi 3 dpi
C57BL/6
SPF 5W
Daily PBS or SKL i.p. injection
m
Competitive index (ΔqseC/WT)
Liver
Spleen
Ileum
Cecal contents
Feces

Fig 7

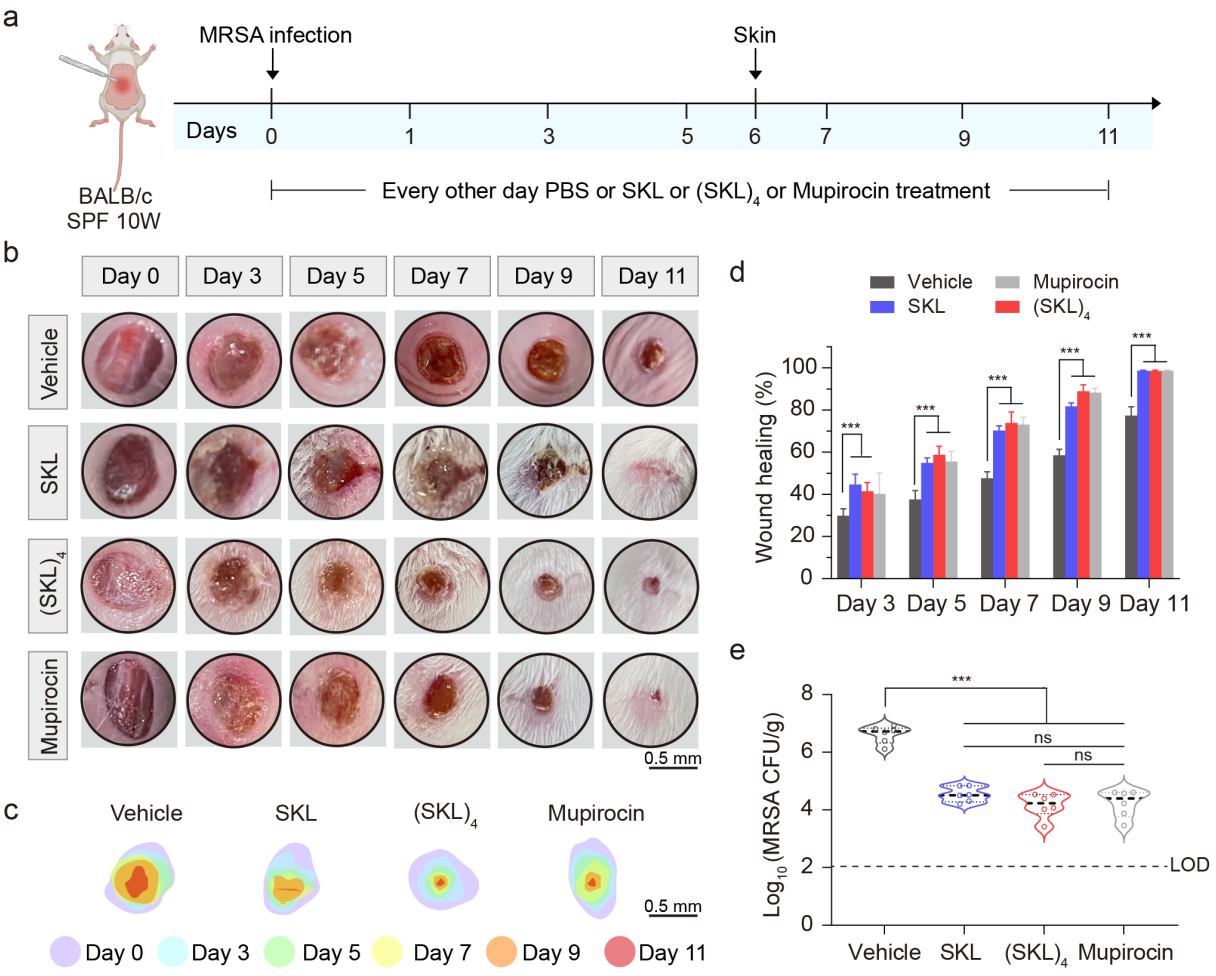
a
MRSA infection
Skin
Days
0
1
3
5
6
7
9
11
BALB/c
SPF 10W
Every other day PBS or SKL or (SKL)4 or Mupirocin treatment
b
Day 0
Day 3
Day 5
Day 7
Day 9
Day 11
Vehicle
SKL
(SKL)4
Mupirocin
0.5 mm
c
Vehicle
SKL
(SKL)4
Mupirocin
0.5 mm
Day 0
Day 3
Day 5
Day 7
Day 9
Day 11
d
Vehicle
SKL
Mupirocin
(SKL)4
Wound healing (%)
Day 3
Day 5
Day 7
Day 9
Day 11
e
Log10 (MRSA CFU/g)
ns
ns
LOD
Vehicle
SKL
(SKL)4
Mupirocin